Journal of Control, Automation and Electrical Systems (2019) 30:741–753
https://doi.org/10.1007/s40313-019-00482-x

Dynamic Analysis of Grid-Connected Droop-Controlled Converters and Synchronverters

Reginaldo V. Ferreira[1] · Sidelmo M. Silva[2] · Hélio M. A. Antunes[3] · Giri Venkataramanan[4]

Received: 30 August 2018 / Revised: 7 February 2019 / Accepted: 1 June 2019 / Published online: 17 June 2019

Abstract
The widespread utilization of micro-sources connected to the power grid, especially in microgrid applications, has led to the development of many different techniques to allow the parallel operation of these sources without communication links. Most of the proposed techniques aim to emulate the behavior of a synchronous generator, as it is the case of the droop control and the synchronverter. The goal of this paper is to develop a unified framework for the study of the dynamics of these two different approaches and to do a comparative analysis of their behavior using steady-state and small-signal models. Even though the mechanics of realization of the two approaches are different, it is shown that their models can be unified in a form that explicitly demonstrates their similarities and differences. The paper presents relationships between the equivalent parameters of the two systems that affect particular dynamic behaviors. Furthermore, it is shown that the differences in their small-signal models are restricted to a single 2×2 matrix. In fact, the 2×2 matrix can be appropriately selected to model different control techniques such as virtual synchronous generators or virtual synchronous machines. The results are validated via MATLAB/Simulink simulations and a hardware-in-the-loop with the micro-source control running in a TMS320F28335 Texas Instruments microcontroller.

Keywords Microgrids · Synchronverters · Droop-controlled converters · Small-signal models

1 Introduction

The last two decades have been experiencing an increasing interest in applications of distributed generation (DG) in electric power systems (Bouzid et al. 2015; Patrao et al. 2015; Blaabjerg et al. 2006; Carrasco et al. 2006; Blaabjerg et al. 2004). With the introduction of the concept of microgrids (Lasseter 2002; Lasseter and Paigi 2004), the integration of DG has been receiving a remarkable attention, with a great number of experimental installations of microgrids implemented around the world (Bouzid et al. 2015; Mariam et al. 2013; Hossain et al. 2014; Pogaku et al. 2007; Guerrero et al. 2007; Sao and Lehn 2008; Krishnamurthy et al. 2008; Kroposki et al. 2008). In order to operate various DGs connected to a power bus, avoiding or minimizing the use of communication links, the utilization of control strategies developed initially for parallel operation of UPS (Uninterruptible Power Systems) has been considered an important alternative (Rocabert et al. 2012; Chandorkar et al. 1993). In this context, the control of the distributed power converter to emulate the operation of synchronous machines has gained increasing popularity (Frack et al. 2015; Chen et al. 2011; Shintai et al. 2014; Coelho et al. 2002). Among the main reasons for the widespread use of these techniques are:

- Well proven capability of parallel connected synchronous machines;
- Possibility to independently control the injection of reactive and active power;
- Possibility to operate parallel machines with different rated parameters;
- Easy power sharing capability.

This paper presents a unified analysis of the operation of the synchronverter and the droop-controlled converter, with

✉ Reginaldo V. Ferreira
reginaldo.ferreira@ifmg.edu.br

[1] Instituto Federal de Educacao Ciencia e Tecnologia de Minas Gerais, Rua Itaguaçu, 595, Betim, MG, Brazil

[2] Universidade Federal de Minas Gerais, Av. Antônio Carlos, 6627, Belo Horizonte, MG, Brazil

[3] Universidade Federal do Espírito Santo, Av. Fernando Ferrari, 514, Vitória, ES, Brazil

[4] WEMPEC, University of Wisconsin, Madison, WI, USA

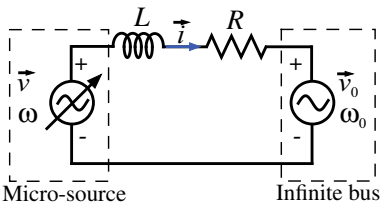

Fig. 1 Schematic diagram of the micro-source connected to an infinite bus

a focus on the small-signal dynamics of a grid-connected converter, as represented in Fig. 1. The simplified schematic representation illustrates a micro-source connected to a power bus through a RL series impedance. For the sake of simplicity, the bus is assumed to have a power rating much greater than the micro-source, such that the operation of this last is not capable of changing the grid frequency (ω_0) or grid voltage magnitude (v_0) of the bus. In addition, the micro-source is modeled initially as an ideal voltage-controlled source. Then, the power converter with its high-frequency dynamics due to the PWM (*pulse-width modulation*) switching, internal filters and voltage and current control loops is included to take into account any influence of these elements on the active and reactive power flow control.

A small-signal model for the system with each control architecture is developed and used to allow a better understanding of the dynamic behavior of the alternatives under parameter variations and disturbances. The small-signal models are validated through simulations using a MATLAB/Simulink and a Typhoon HIL model, with the micro-source control running in a Texas Instruments TMS320F28335 microcontroller. Once the small-signal models are validated, they are used to access information on the dynamic operation of the systems for more general operating conditions. The unified approach used to develop the small-signal models can also be used to model other algorithms that mimic the synchronous machine operation. It is also shown that the models developed could be used even for large- signal excursions with acceptable errors.

The main contributions of the paper are:

- An unified approach to model synchronverters, droop and other virtual synchronous machine control strategies for small-signal analysis;
- A parameter comparison of the droop control converter and the synchronverter, including both active and reactive control loops;
- A unified small-signal model framework to model the droop control, synchronverter and other control algorithms that mimic the operation of a synchronous generator, including the currents dynamics;
- A closer view on the similarities and differences between the droop-controlled converter and synchronverter;
- Information on the couplings between active and reactive power in the droop and synchronverter control;
- Presentation of the fact that for a given set of equivalent parameters, the synchronverter has a wider stability margin than the droop-controlled converter, considering variations on the voltage magnitude gain.

2 Droop-Controlled Micro-source Converter

The micro-source considered in this study is assumed to operate with a frequency ω and a voltage magnitude v, which are based on the droop control strategy (Coelho et al. 2002; Chandorkar et al. 1993; Moslemi and Mohammadpour 2015; Kawabata and Higashino 1988; Mendoza-araya 2014; Lee et al. 2009; Majumder et al. 2010; Tayab et al. 2017; Brabandere et al. 2005; Guerrero et al. 2007; Wen et al. 2016; Liu et al. 2016).

As illustrated in Fig. 2, the droop-controlled micro-source varies its frequency and voltage magnitude based on the active (p) and reactive (q) power at its terminals, with a voltage droop gain (K_q) and a frequency droop gain (K_p). The idea behind the droop control is the emulation of a synchronous machine connected to a power bus through a purely inductive line. For resistive or RL power lines, a transformation applied on the measured active and reactive power is proposed in Brabandere et al. (2005), prior to the application of the droop gains, in order to the decouple the active and reactive power channels. In the present work, the R/L relation is considered very small and the coupling and the transformations of the measured powers are not considered.

In Fig. 2, P^* is the active power that the micro-source has to inject when operating at frequency Ω^*, and Q^* is the reactive power to be injected when operating with a voltage

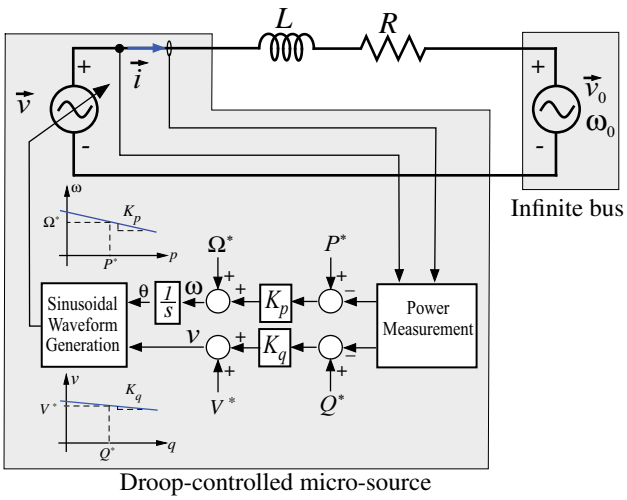

Fig. 2 Schematic diagram of the droop-controlled micro-source

magnitude equal to V^*. The *Sinusoidal Waveform Generation* block is responsible for generating the three-phase voltages, based on the voltage vector angle (θ) and magnitude (v).

Using a vector representation for the three-phase variables (Novotny and Lipo 1996), the vector quantities of Fig. 2 can be written as:

$$\mathbf{v} = v_d + jv_q \tag{1}$$
$$\mathbf{v}_0 = v_{0d} + jv_{0q} \tag{2}$$
$$\mathbf{i} = i_d + ji_q \tag{3}$$

where subscripts d and q stand for the direct and quadrature axis components of the vectors quantities in a synchronous rotating frame.

The circuit equation for the system in the vector form is:

$$\mathbf{v} - \mathbf{v}_0 = [(s + j\omega)L + R]\mathbf{i} \tag{4}$$

In the vector form, the term $j\omega$ has to be added to the derivative Laplace symbol s to represent the cross-couplings between the d and q axes variables.

The magnitude and angle of the micro-source voltage vector are, respectively:

$$v = |\mathbf{v}| = \sqrt{v_d^2 + v_q^2} \tag{5}$$
$$\theta = \arctan\left(\frac{v_q}{v_d}\right) \tag{6}$$

In the time domain, (4) can be rewritten for the d-axis and q-axis components as:

$$\frac{\mathrm{d}i_d}{\mathrm{d}t} = \frac{1}{L}(v_d - v_{0d} - Ri_d + \omega Li_q) \tag{7}$$
$$\frac{\mathrm{d}i_q}{\mathrm{d}t} = \frac{1}{L}(v_q - v_{0q} - Ri_q - \omega Li_d) \tag{8}$$

The active and reactive power at the micro-source terminals can be expressed as:

$$p = \frac{3}{2}(v_d i_d + v_q i_q) \tag{9}$$
$$q = \frac{3}{2}(v_q i_d - v_d i_q) \tag{10}$$

A first-order low-pass filter with a cutoff frequency equal to ω_f is commonly included in the power measurement of the droop-controlled micro-source, as expressed by:

$$p_\mathrm{f}(s) = \frac{\omega_\mathrm{f}}{s + \omega_\mathrm{f}} p(s) \tag{11}$$
$$q_\mathrm{f}(s) = \frac{\omega_\mathrm{f}}{s + \omega_\mathrm{f}} q(s) \tag{12}$$

From Fig. 2, the frequency and voltage droop equations can be written as:

$$\omega = \Omega^* - K_p(p_\mathrm{f} - P^*) \tag{13}$$
$$v = V^* - K_q(q_\mathrm{f} - Q^*) \tag{14}$$

Building upon the traditional droop control presented here, many different variations have been proposed to improve the operation of the droop-controlled converter, including (Zhang et al. 2014; Skjellnes et al. 2002; Rowe and Summers 2013; Moslemi and Mohammadpour 2015). While the methodology developed here can also be used to deal with different control strategies with minor modifications, these techniques are considered to be out of the scope of this work, in order to maintain the tight focus of this paper.

3 Synchronverter: Principle of Operation

The concept of the synchronverter was first introduced in Zhong et al. (2011) in an attempt to mimic the dynamic behavior of synchronous machines connected to the power grid, through the use of power electronic converters. Since then, many efforts have been developed to better understand the synchronverter behavior and to improve its dynamic response (Zhang et al. 2013; Ma et al. 2012; Zhong et al. 2014), in addition to adaptations for single-phase applications (Mishra et al. 2016; Ferreira et al. 2016). Figure 3 shows an schematic diagram of the synchronverter. While it appears to be different from the schematic diagram proposed in Zhong et al. (2011), the model presented here uses the variables represented in the DQ reference frame, for the sake of simplicity and model unification. This approach enables a straightforward comparison with the droop control scheme, presented in Fig. 2.

In Fig. 3, J is the emulated moment of inertia, D_p is the emulated damping coefficient, D_q is the voltage droop coefficient, and K is a constant used to calculate the flux linkage (λ_f) of the virtual machine. Also, in the figure, one can note the presence of a block ($abc - dq$) responsible for transforming the three-phase voltages and currents to a synchronous rotating reference frame, aligned with the d-axis voltage component of the generator voltage. By doing this, the q-axis voltage (v_q) component will be zero and the active and reactive power will be functions of the direct (i_d) and quadrature (i_q) current components, respectively, besides the d-axis voltage (v_d) component. The function of the *Sinusoidal Waveform Generator* block is the same as for the droop control algorithm, shown in Fig. 2.

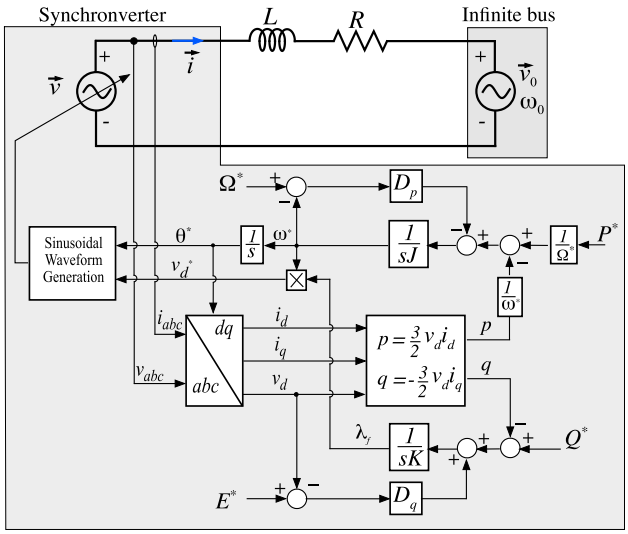

Fig. 3 Schematic diagram of the synchronverter represented in DQ reference frame

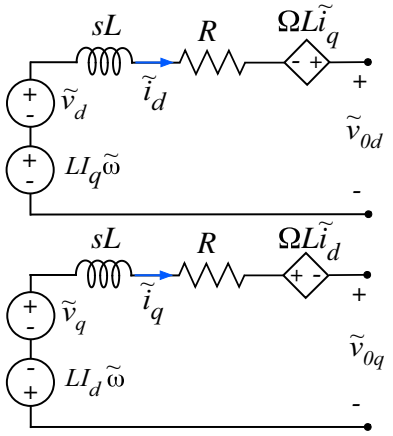

Fig. 4 Linearized DQ equivalent circuit of the micro-source connected to an infinite bus

4 Small-Signal Models

In this section, small-signal models for the droop-controlled converter and the synchronverter connected to an infinite bus are developed. A similar approach based on a synchronously rotating reference frame is used for both systems, aiming an easier comparison of the resultant small-signal models.

4.1 Droop-Controlled Converter

In Coelho et al. (2002), a small-signal model of a droop-controlled source was developed. However, it was assumed that the frequency variations were negligible and the effect of these variations on the line impedances was not considered. It is important to emphasize that although frequency variation in power systems is usually small, the effect of these variations must be taken into account for a more complete understanding of the dynamics of the system, as it will be shown below.

If we account for the frequency variations in (7) and (8), these equations become nonlinear due to the current–frequency product.

Linearizing (7) and (8), one can obtain:

$$\frac{\mathrm{d}\tilde{i}_d}{\mathrm{d}t} = \frac{1}{L}(\tilde{v}_d - \tilde{v}_{0d}) - \frac{R}{L}\tilde{i}_d + \Omega\tilde{i}_q + I_q\tilde{\omega} \tag{15}$$

$$\frac{\mathrm{d}\tilde{i}_q}{\mathrm{d}t} = \frac{1}{L}(\tilde{v}_q - \tilde{v}_{0q}) - \frac{R}{L}\tilde{i}_q - \Omega\tilde{i}_d - I_d\tilde{\omega} \tag{16}$$

where the accent $\tilde{}$ is used to denote variables with a small variation around an operating point. In addition, throughout this work, uppercase letters are used for constants and stand-still values of the variables in the operating point.

From (15) and (16), it is possible to draw the linearized DQ equivalent circuit of the micro-source connected to an infinite bus, as illustrated in Fig. 4. Observe the inclusion of a term that accounts for the effect of the frequency variations on the currents of the system. This term is essential for a more complete modeling of the micro-source.

Linearizing (5), one can obtain:

$$\tilde{v} = n_d\tilde{v_d} + n_q\tilde{v_q} \tag{17}$$

where:

$$n_d = \frac{V_d}{\sqrt{V_d^2 + V_q^2}} = \frac{V_d}{V} \tag{18}$$

$$n_q = \frac{V_q}{\sqrt{V_d^2 + V_q^2}} = \frac{V_q}{V} \tag{19}$$

The linearization of (6) leads to:

$$\tilde{\theta} = m_d\tilde{v_d} + m_q\tilde{v_q} \tag{20}$$

where:

$$m_d = \frac{-V_q}{V_d^2 + V_q^2} = \frac{-V_q}{V^2} \tag{21}$$

$$m_q = \frac{V_d}{V_d^2 + V_q^2} = \frac{V_d}{V^2} \tag{22}$$

Differentiating (17) and (20), one can obtain:

$$\dot{\tilde{v}} = n_d\dot{\tilde{v}}_d + n_q\dot{\tilde{v}}_q \tag{23}$$

$$\dot{\tilde{\theta}} = \tilde{\omega} = m_d\dot{\tilde{v}}_d + m_q\dot{\tilde{v}}_q \tag{24}$$

For small-signal quantities, (13) and (14) become:

$$\tilde{\omega} = \omega - \Omega^* = -K_p(p_\mathrm{f} - P^*) = -K_p\tilde{p}_\mathrm{f} \tag{25}$$
$$\tilde{v} = v - V^* = -K_q(q_\mathrm{f} - Q^*) = -K_q\tilde{q}_\mathrm{f} \tag{26}$$

The use of (11) and (12) in (25) and (26) yields:

$$\frac{\mathrm{d}\tilde{\omega}}{\mathrm{d}t} = -\omega_\mathrm{f}\tilde{\omega} - K_p\omega_\mathrm{f}\tilde{p} \tag{27}$$
$$\frac{\mathrm{d}\tilde{v}}{\mathrm{d}t} = -\omega_\mathrm{f}\tilde{v} - K_q\omega_\mathrm{f}\tilde{q} \tag{28}$$

Using (17)–(28) and after manipulations, it is possible to obtain:

$$\dot{\tilde{v}}_d = -V_q\tilde{\omega} - \frac{\omega_\mathrm{f}V_d^2}{V^2}\tilde{v}_d - \frac{\omega_\mathrm{f}V_dV_q}{V^2}\tilde{v}_q - \frac{\omega_\mathrm{f}K_qV_d}{V}\tilde{q} \tag{29}$$
$$\dot{\tilde{v}}_q = V_d\tilde{\omega} - \frac{\omega_\mathrm{f}V_dV_q}{V^2}\tilde{v}_d - \frac{\omega_\mathrm{f}V_q^2}{V^2}\tilde{v}_q - \frac{\omega_\mathrm{f}K_qV_q}{V}\tilde{q} \tag{30}$$

Linearization of (9) and (10) leads to:

$$\tilde{p} = \frac{3}{2}\left(V_d\tilde{i}_d + I_d\tilde{v}_d + V_q\tilde{i}_q + I_q\tilde{v}_q\right) \tag{31}$$
$$\tilde{q} = \frac{3}{2}\left(V_q\tilde{i}_d + I_d\tilde{v}_q - V_d\tilde{i}_q - I_q\tilde{v}_d\right) \tag{32}$$

In a matrix form, (15) and (16) can be rewritten as:

$$\begin{bmatrix}\tilde{v}_d\\ \tilde{v}_q\end{bmatrix} - \begin{bmatrix}\tilde{v}_{0d}\\ \tilde{v}_{0q}\end{bmatrix} = \begin{bmatrix}(sL+R) & -\Omega L\\ \Omega L & (sL+R)\end{bmatrix}\begin{bmatrix}\tilde{i}_d\\ \tilde{i}_q\end{bmatrix} + \begin{bmatrix}-LI_q\\ LI_d\end{bmatrix}[\tilde{\omega}] \tag{33}$$

In (33), the large-signal impedance matrix of the system is:

$$\mathbf{Z_0} = \begin{bmatrix}(sL+R) & -\Omega L\\ \Omega L & (sL+R)\end{bmatrix} \tag{34}$$

where boldface characters represent matrix quantities.

From (33), if the micro-source voltage and the bus voltage variations are set to zero, one can obtain:

$$\mathbf{Z_0}\begin{bmatrix}\tilde{i}_d\\ \tilde{i}_q\end{bmatrix} = \begin{bmatrix}LI_q\\ -LI_d\end{bmatrix}[\tilde{\omega}] \tag{35}$$

From (35), solving for $\tilde{i}_d$ and $\tilde{i}_q$ yields:

$$\tilde{i}_d(s) = -\frac{1}{\Omega L}\left[(sL+R)\tilde{i}_q + LI_d\tilde{\omega}\right] \tag{36}$$
$$\tilde{i}_q(s) = \frac{1}{\Omega L}\left[(sL+R)\tilde{i}_d - LI_q\tilde{\omega}\right] \tag{37}$$

Using (36) and (37) in (35), it is possible to obtain a relation that expresses the impact of the frequency variation on the circuit currents, as:

$$\frac{\tilde{i}_d(s)}{\tilde{\omega}(s)} = \frac{-(s+R/L)I_q - \Omega I_d}{\left[(s+R/L)^2 + \Omega^2\right]} \tag{38}$$
$$\frac{\tilde{i}_q(s)}{\tilde{\omega}(s)} = \frac{(s+R/L)I_d - \Omega I_q}{\left[(s+R/L)^2 + \Omega^2\right]} \tag{39}$$

In a matrix form, (38) and (39) are expressed as:

$$\begin{bmatrix}\tilde{i}_d(s)\\ \tilde{i}_q(s)\end{bmatrix} = \begin{bmatrix}\frac{-(s+R/L)I_q-\Omega I_d}{\left[(s+R/L)^2+\Omega^2\right]}\\ \\ \frac{(s+R/L)I_d-\Omega I_q}{\left[(s+R/L)^2+\Omega^2\right]}\end{bmatrix}[\tilde{\omega}] = \mathbf{G_{i!}}[\tilde{\omega}] \tag{40}$$

From (31) and (32), a matrix representation for the active and reactive powers can be written as:

$$\tilde{\mathbf{S}} = \begin{bmatrix}\tilde{p}\\ \tilde{q}\end{bmatrix} = \frac{3}{2}\begin{bmatrix}V_d & V_q\\ V_q & -V_d\end{bmatrix}\begin{bmatrix}\tilde{i}_d\\ \tilde{i}_q\end{bmatrix} + \frac{3}{2}\begin{bmatrix}I_d & I_q\\ -I_q & I_d\end{bmatrix}\begin{bmatrix}\tilde{v}_d\\ \tilde{v}_q\end{bmatrix} \tag{41}$$

For the sake of simplification, we define matrices:

$$\mathbf{V_{dq}} = \frac{3}{2}\begin{bmatrix}V_d & V_q\\ V_q & -V_d\end{bmatrix} \tag{42}$$
$$\mathbf{I_{dq}} = \frac{3}{2}\begin{bmatrix}I_d & I_q\\ -I_q & I_d\end{bmatrix} \tag{43}$$

From (17) and (20) and after manipulations, one can write:

$$\tilde{v}_d = \frac{V_d}{V}\tilde{v} - V_q\tilde{\theta} \tag{44}$$
$$\tilde{v}_q = -\frac{V_q}{V}\tilde{v} + V_d\tilde{\theta} \tag{45}$$

Recalling that $\tilde{\omega} = s\tilde{\theta}$, (44) and (45) can be written in a matrix form as:

$$\begin{bmatrix}\tilde{v}_d\\ \\ \tilde{v}_q\end{bmatrix} = \begin{bmatrix}-\frac{V_q}{s} & \frac{V_d}{V}\\ \\ \frac{V_d}{s} & -\frac{V_q}{V}\end{bmatrix}\begin{bmatrix}\tilde{\omega}\\ \\ \tilde{v}\end{bmatrix} = \mathbf{G_{rp}}\begin{bmatrix}\tilde{\omega}\\ \\ \tilde{v}\end{bmatrix} \tag{46}$$

The frequency variations can be also represented in a matrix form, based on the definition developed above, as:

$$[\tilde{\omega}] = [1\ \ 0]\begin{bmatrix}\tilde{\omega}\\ \tilde{v}\end{bmatrix} = \mathbf{G_\omega}\begin{bmatrix}\tilde{\omega}\\ \tilde{v}\end{bmatrix} \tag{47}$$

Writing the droop gains and the low-pass filter in a matrix form leads to:

$$\begin{bmatrix}\tilde{\omega}\\ \tilde{v}\end{bmatrix} = \begin{bmatrix}-K_p\frac{\omega_\mathrm{f}}{(s+\omega_\mathrm{f})} & 0\\ 0 & -K_q\frac{\omega_\mathrm{f}}{(s+\omega_\mathrm{f})}\end{bmatrix}\begin{bmatrix}\tilde{p}\\ \tilde{q}\end{bmatrix} = \mathbf{G_d}\begin{bmatrix}\tilde{p}\\ \tilde{q}\end{bmatrix} \tag{48}$$

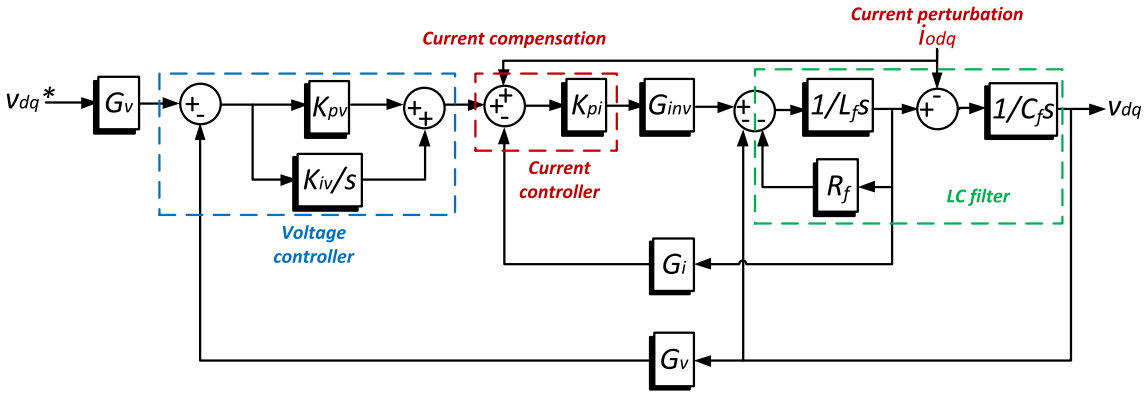

Fig. 5 Block diagram of inverter inner control, including the LC filter behavior

Once the small-signal model for the droop-controlled micro-source is now available, it is possible to include the dynamics of the control loop of the converter LC filter. Figure 5 presents the block diagram of the voltage and current control loops of the converters. In the voltage loop, a proportional+integral (PI) controller is used. For the current control loop, a proportional (P) controller is applied. In this figure, G_v is the voltage sensor gain, G_i is the current sensor gain, K_{pv} and K_{iv} are the proportional and integral gains of the voltage loop, K_{pi} is the proportional gain in current loop, G_{inv} is the converter gain, and L_{f}, R_{f} and C_{f} are the inductance, inductor resistance and capacitance of the LC output filter.

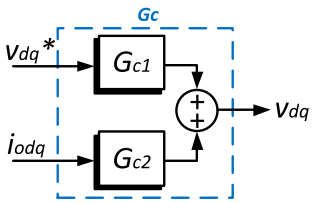

Fig. 6 DQ small-signal representation of the control of the output filter

It is important to highlight that G_c is a ratio between the output voltage and the voltage reference to the inverter. So, this equation results in a dq output voltage to be converted to $\tilde{\omega}$, $\tilde{v}$, using matrix (52).

$$\tilde{v}_{dq_1} = \frac{\frac{G_v.K_{\mathrm{pv}}.K_{\mathrm{pi}}.G_{\mathrm{inv}}}{C_{\mathrm{f}}L_{\mathrm{f}}}.s + \frac{G_v.K_{\mathrm{iv}}.K_{\mathrm{pi}}.G_{\mathrm{inv}}}{C_{\mathrm{f}}L_{\mathrm{f}}}}{s^3 + \left(\frac{R_{\mathrm{f}}}{L_{\mathrm{f}}} + \frac{K_{\mathrm{pi}}.G_{\mathrm{inv}}.G_i}{L_{\mathrm{f}}}\right).s^2 + \frac{G_v.K_{\mathrm{pv}}.K_{\mathrm{pi}}.G_{\mathrm{inv}}}{C_{\mathrm{f}}L_{\mathrm{f}}} + \frac{G_v.K_{\mathrm{iv}}.K_{\mathrm{pi}}.G_{\mathrm{inv}}}{C_{\mathrm{f}}L_{\mathrm{f}}}}.\tilde{v}^*_{dq} = \mathbf{G_{c1}}.\tilde{v}^*_{dq} \tag{49}$$

$$\tilde{v}_{dq_2} = \frac{-L_{\mathrm{f}}s^2 - R_{\mathrm{f}}s}{s^3 + \left(\frac{R_{\mathrm{f}}}{L_{\mathrm{f}}} + \frac{K_{\mathrm{pi}}.G_{\mathrm{inv}}.G_i}{L_{\mathrm{f}}}\right).s^2 + \frac{G_v.K_{\mathrm{pv}}.K_{\mathrm{pi}}.G_{\mathrm{inv}}}{C_{\mathrm{f}}L_{\mathrm{f}}} + \frac{G_v.K_{\mathrm{iv}}.K_{\mathrm{pi}}.G_{\mathrm{inv}}}{C_{\mathrm{f}}L_{\mathrm{f}}}}.\tilde{i}_{o_{dq}} = \mathbf{G_{c2}}.\tilde{i}_{o_{dq}} \tag{50}$$

Figure 5 also presents the output currents of the micro-source ($i_{o_{dq}}$), which act as perturbations for the control loops, and the voltage references v^*_{dq} from the droop or synchronverter control algorithms, which act as set points for the voltage control loop.

From the block diagram of Fig. 5, it is possible to obtain the two transfer functions relating the filter output voltages with the set point and disturbance of the control system, as presented in (49) and (50). Both contributions are added to obtain v_{dq} as illustrated in Fig. 6. Equation (51) presents these relations in a matrix form.

$$\tilde{v}_{dq} = \begin{bmatrix} G_{c1} & G_{c2} \end{bmatrix} \begin{bmatrix} \tilde{v}^*_{dq} \\ \tilde{i}_{o_{dq}} \end{bmatrix} \tag{51}$$

$$\mathbf{G_{pr}} = \frac{1}{V_d^2 - V_q^2} \begin{bmatrix} V_q.s & V_d.s \\ V_d.V & V_q.V \end{bmatrix} \tag{52}$$

Using the matrix representation of the developed small-signal models, it is possible to obtain a block diagram representation for the system, as shown in Fig. 7.

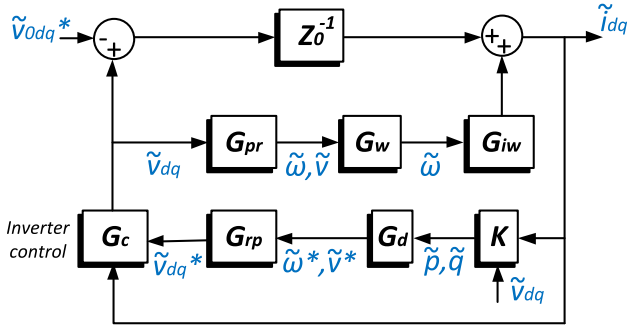

Fig. 7 DQ small-signal block diagram of the micro-source

From Fig. 7, the transfer function relating small variations in the bus terminal voltage with the variations in the micro-source currents can be obtained. This relation is the small-signal output impedance of the droop-controlled micro-source, given by:

$$\frac{\tilde{\mathbf{v}}_{\mathbf{0_{dq}}}(\mathbf{s})}{\tilde{\mathbf{i}}_{\mathbf{dq}}(\mathbf{s})} = \mathbf{G_{vi}}(\mathbf{I} + \mathbf{Z_0}\mathbf{G_{pr}}\mathbf{G_\omega}\mathbf{G_{i\omega}}) - \mathbf{Z_0} \tag{53}$$

where:

$$\mathbf{G_{vi}} = \frac{\mathbf{G_{C1}}\mathbf{G_{rp}}\mathbf{G_d}\mathbf{V_{dq}} + \mathbf{G_{C2}}}{\mathbf{I} - \mathbf{G_{C1}}\mathbf{G_{rp}}\mathbf{G_d}\mathbf{I_{dq}}} \tag{54}$$

$$\mathbf{Z_{ss}}(s) = \frac{\tilde{\mathbf{v}}_{\mathbf{0_{dq}}}(\mathbf{s})}{\tilde{\mathbf{i}}_{\mathbf{dq}}(\mathbf{s})} = \begin{bmatrix} Z_{dd}(s) & Z_{qd}(s) \\ Z_{dq}(s) & Z_{qq}(s) \end{bmatrix} \tag{55}$$

Equation (55) gives the small-signal impedances from channels d and q to channels d and q.

4.2 Synchronverter

In Wei et al. (2015), a small-signal model of a synchronverter was developed. However, in the adopted approach, it was not taken into account the droop gain to regulate the voltage magnitude. A modeling based on an abc reference also did not contribute very much to the understanding of the similarities and differences between the droop control and the synchronverter.

Most of the previous development presented here for the small-signal model of the droop-controlled converter can also be applied to obtain the small-signal model of the synchronverter. Specifically, if we look at Fig. 7, it is possible to note that excluding the Control Matrix (G_d) of the droop control, all the other elements can also be used to model the synchronverter connected to the infinite bus, since they deal with the model of the system without its control. The analysis of Fig. 3 allows us to obtain a relation between the small-signal active and reactive powers and the small-signal frequency and voltage variations for the synchronverter as:

$$\begin{bmatrix} \tilde{\omega} \\ \tilde{v} \end{bmatrix} = \begin{bmatrix} -\frac{1}{\Omega}\frac{1}{(sJ+D_p)} & 0 \\ \frac{A_f}{\Omega}\frac{1}{(sJ+Dp)} & -\frac{1}{(\frac{sK}{\Omega}+D_q)} \end{bmatrix} \begin{bmatrix} \tilde{p} \\ \tilde{q} \end{bmatrix} = \mathbf{G_s} \begin{bmatrix} \tilde{p} \\ \tilde{q} \end{bmatrix} \tag{56}$$

By the use of matrix $\mathbf{G_s}$ as the Control Matrix in Fig. 7, one can obtain a small-signal model for the synchronverter.

It is worthy of note that (53)–(55) also can be used to calculate the small-signal impedances and/or admittance of the synchronverter, if matrix $\mathbf{G_d}$ is replaced by $\mathbf{G_s}$.

5 Synchronverter and Droop Parameters Relations

Comparing the nonzero elements of matrices $\mathbf{G_d}$ and $\mathbf{G_s}$, it is possible to determine the parameter values for the droop control and the synchronverter that would give them a closer dynamic response. For the frequency droop gain, one can obtain:

$$K_p = \frac{1}{D_p\Omega} \rightarrow D_p = \frac{1}{K_p\Omega} \tag{57}$$

For the cutoff frequency of the low-pass filter, we get:

$$\frac{1}{\omega_f} = \frac{J}{D_p} \rightarrow J = \frac{D_p}{\omega_f} \tag{58}$$

$$\frac{1}{\omega_f} = \frac{K}{\Omega D_q} \rightarrow K = \frac{\Omega D_q}{\omega_f} \tag{59}$$

For the magnitude droop gain, we obtained:

$$K_q = \frac{1}{D_q} \tag{60}$$

According to Zhong et al. (2011), J and K are calculated through:

$$J = \tau_f D_p \tag{61}$$

$$K = \tau_v \omega_n D_q \tag{62}$$

where τ_f and τ_v are the frequency and voltage droop time constants, respectively. From the previous equations, it is possible to express:

$$\tau_f = \tau_v = \frac{1}{\omega_f} \tag{63}$$

For the sake of simplicity, in the present work, these time constants are considered equal and the filters in the measurement of the active and reactive powers of the droop control algorithm have the same time constants. It is worthy to note that the low-pass filter commonly used in the power measurement of droop-controlled converters adds the effect of

Table 1 Droop and synchronverter parameter relations

Control loop	Droop	Synchronverter	
Frequency	K_p	$D_p = \frac{1}{\Omega K_p}$	$J = \tau_f D_p$
	ω_f	$\tau_f = \frac{1}{\omega_f}$	
Voltage	K_q	$D_q = \frac{1}{K_q}$	$K = \tau_v \Omega D_q$
	ω_f	$\tau_v = \frac{1}{\omega_f}$	

Table 2 Base parameters for simulations

	Value	Units
Electrical parameters		
System frequency (f_0)	60	Hz
Infinite bus voltage magnitude (V_0)	$127\sqrt{2}$	V
Infinite bus voltage angle	0	rad
Line resistance (R)	15	mΩ
Line inductance (L)	710	μH
Micro-source voltage magnitude (V)	$127\sqrt{2}$	V
Micro-source voltage angle	0.01	rad
Capacitance of the filter (C_f)	411	μF
Inductance of the filter (L_f)	171	μH
Resistance of the filter (R_f)	6.4	mΩ
Control parameters		
Frequency droop gain (K_p)	0.05	%
Voltage droop gain (K_q)	0.01	%
Frequency of the low-pass filter (ω_f)	6	Hz
Proportional voltage gain (K_{pv})	1.9	–
Integral voltage gain (K_{iv})	10	–
Proportional current gain (K_{pi})	0.13	–
Switching frequency (f_{sw})	6k	Hz

a virtual inertia to this control strategy, which could also be varied for increased flexibility.

Another interesting remark when comparing matrices $\mathbf{G_d}$ and $\mathbf{G_s}$ is that the droop-controlled micro-source can be seen as a particular case of the synchronverter when element G_{s21} is equal to zero and the equivalence of parameters of Table 1 is considered.

6 Validation of the Small-Signal Models

To validate the small-signal models of the droop-controlled micro-source and the synchronverter, dynamic models for both systems were implemented in MATLAB/Simulink. The parameters used in the simulations are presented in Table 2.

A set of simulations was conducted using the small-signal and the dynamic models with these parameters.

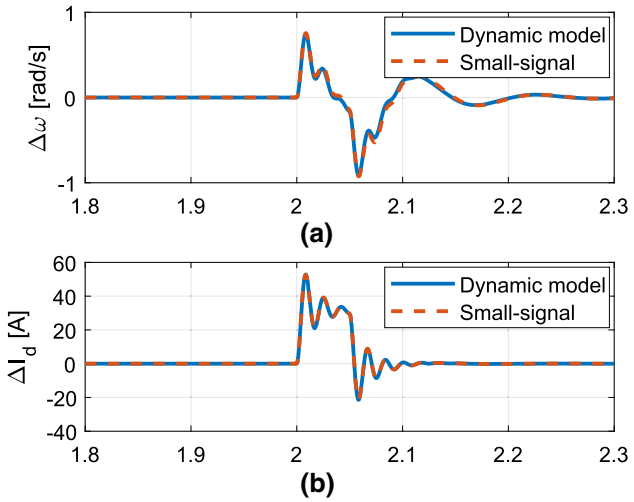

Fig. 8 Dynamic response of the droop-controlled micro-source under a 5% disturbance in the d-axis component of the bus voltage for 50 ms

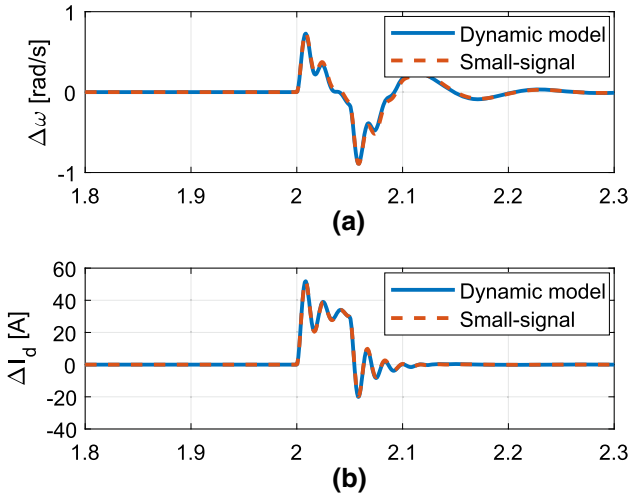

Fig. 9 Dynamic response of the synchronverter under a 5% disturbance in the d-axis component of the bus voltage for 50 ms

Figures 8, 9 and 10 show the transient response of the droop-controlled micro-source and the synchronverter from the dynamic and small-signal models, after a variation of the infinite bus voltage. The d-axis component of the bus voltage was increased by 5% for 50 ms. The frequency droop gain (K_p) was set to 0.05%, the voltage droop gain (K_q) was set to 0.01%, and the cutoff frequency of the low-pass filter (w_f) was set to 6 Hz. The parameters of the synchronverter were calculated from these values using the expressions listed in Table 1. Figure 8 shows the results for the droop-controlled converter, while Fig. 9 presents the results for the synchronverter. In Fig. 10, it is possible to compare the results for both control strategies. For all the cases, figure (a) shows the variation of the micro-source frequency ($\tilde{\omega}$), and figure (b) the variation of the micro-source d-axis current ($\tilde{i}_d$).

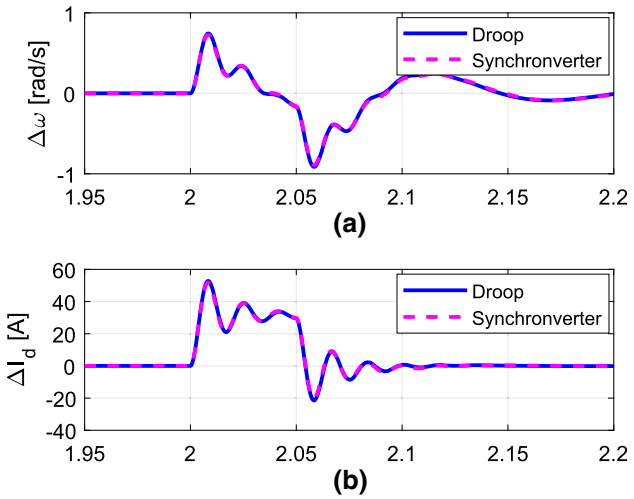

Fig. 10 Dynamic responses of the synchronverter and the droop-controlled micro-source under a 5% disturbance in the d-axis component of the bus voltage for 50 ms

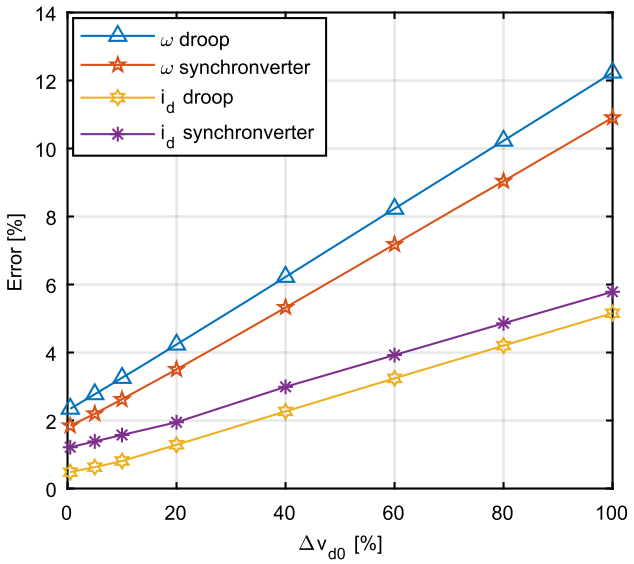

Fig. 11 Percentage errors of the small-signal models compared with the dynamic model. Droop control and synchronverter

As illustrated in Figs. 8 and 9 , there is a good agreement in the results of the dynamic models and the small-signal models for both the droop-controlled micro-source and the synchronverter.

Many other simulations with different gains were conducted in order to validate the small-signal models. The results obtained closely match the results from the dynamic models and due to space limitations are not shown here.

Figure 11 presents the maximum percentage error of the small-signal models compared with the dynamic models for both the droop-controlled micro-source and synchronverter. As illustrated, the small-signal models can reasonably well predict the behavior of the dynamic systems, even in case of large-signal variations. In this figure, one can see that for a variation in the d-axis component of the bus voltage equal to 100%, the maximum errors in the small-signal variables are around 12% for frequency and 6% for currents.

7 Small-Signal Dynamic Behavior of the Synchronverter and the Droop-Controlled Converter

Figure 12 shows the closed-loop poles of the droop-controlled micro-source and synchronverter in the complex plane for the same parameters as used in Section 6. As illustrated, the closed-loop poles of both systems are very similar for the considered parameters.

Figure 13 presents the variation of the closed-loop poles on the complex plane for the droop-controlled converter and the synchronverter, as a function of the increase on gain K_p (0.01–0.9%). This range of variation on K_p leads the droop-controlled converter into instability, illustrating the fact that this control algorithm presents a narrower stable range of values for K_p, compared to the synchronverter. For the present conditions, the critical value of K_p that leads the droop-controlled converter into instability is $K_p = 0.6\%$, while for the synchronverter is $K_p = 1.4\%$.

Figure 14 shows the variation of the closed-loop poles in the complex plane for the droop-controlled converter and the synchronverter, as a function of the increase on gain K_q (0.01–0.2%). As one can see, an increase on gain K_q affects almost identically the closed-loop poles of the droop-controlled converter and the synchronverter.

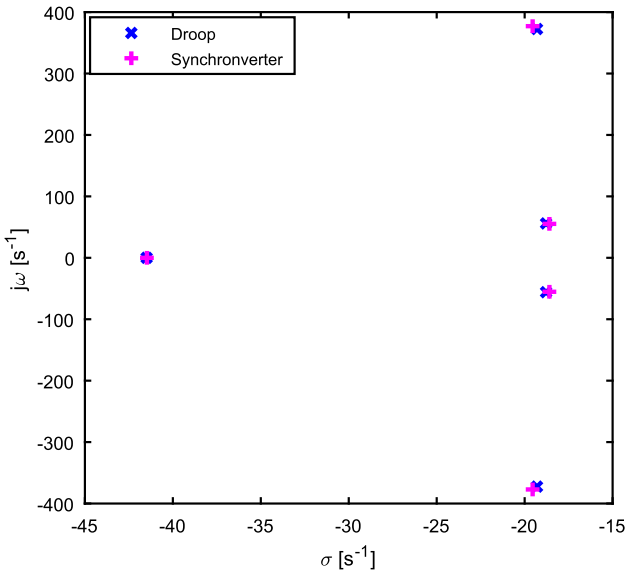

Fig. 12 Poles of the DQ small-signal model on the complex plane ($K_p = 0.05\%$ and $K_q = 0.01\%$). Droop control and synchronverter

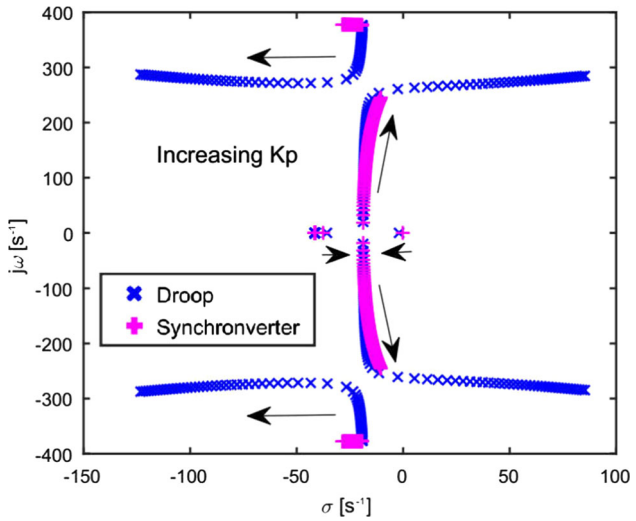

Fig. 13 Poles of the DQ small-signals model on the complex plane as a function of the gain K_p (0.01–0.9%), $K_q = 0.01\%$. Droop control and synchronverter

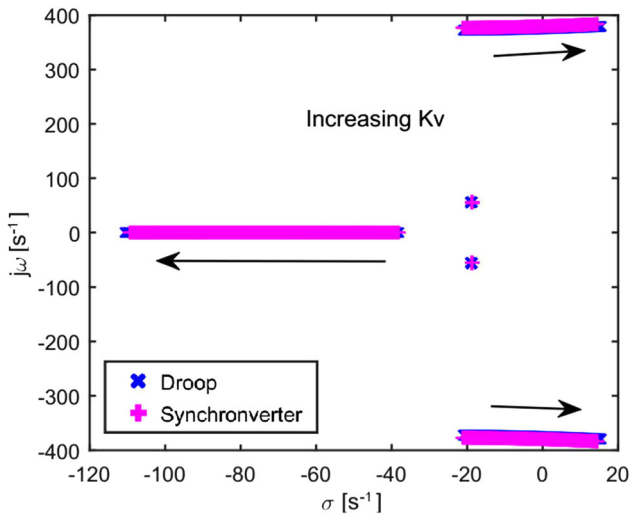

Fig. 14 Poles of the DQ small-signal model on the complex plane as a function of the gain K_q (0.01–0.2%), $K_p = 0.05\%$. Droop control and synchronverter

Figure 15 presents the small-signal admittance of the droop-controlled micro-source and the synchronverter.

8 Experimental Results

Experimental results were obtained from a hardware-in-the-loop model implemented in a Typhoon HIL 600. A TMS320F28335 Texas Instruments microcontroller was used for the control part. Since the results from the droop-controlled converter and the synchronverter are similar, only the response of the latter will be presented.

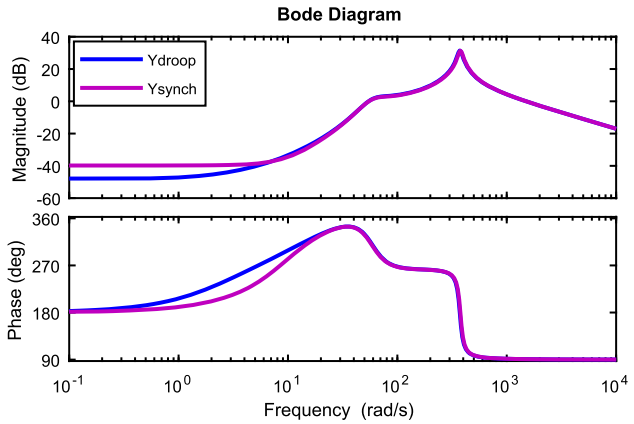

Fig. 15 Small-signal admittance of the droop-controlled converter and the synchronverter from channel d to channel d (Y_{dd}). $K_p = 0.05\%$. Droop control and synchronverter

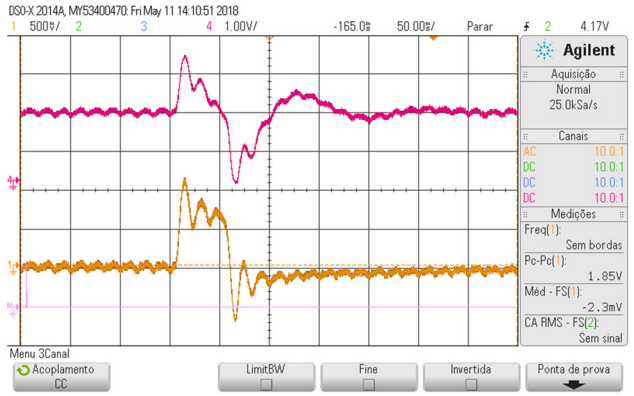

Fig. 16 Experimental result for the synchronverter: frequency and i_d current under a 5% disturbance in the d-axis component of the bus voltage for 50 ms

The parameters used in the HIL model were the same as the ones used in the simulations. In addition, the same disturbance was also considered. Figure 16 shows the frequency and current (i_d) response of the system during the disturbance.

Figures 17 and 18 illustrate the experimental and the small-signal model responses for the frequency and the d-axis current (i_d) under the disturbance. The curves presented in this figure clearly validate the developed small-signal models.

To evaluate the behavior of the converter against small variations in the active power, an experimental result was obtained, in which ΔP is the input signal and the frequency is the output signal. In this scenario, the active power variation is 2 kW during 50 ms. Figure 19 presents the results. One more time, the dynamic response of the experimental setup and the small-signal model is similar.

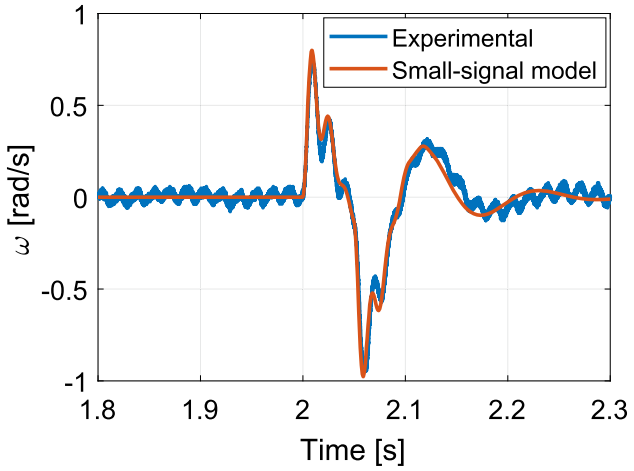

Fig. 17 Small signal x experimental synchronverter result: frequency under a 5% disturbance in the d-axis component of the bus voltage for 50 ms

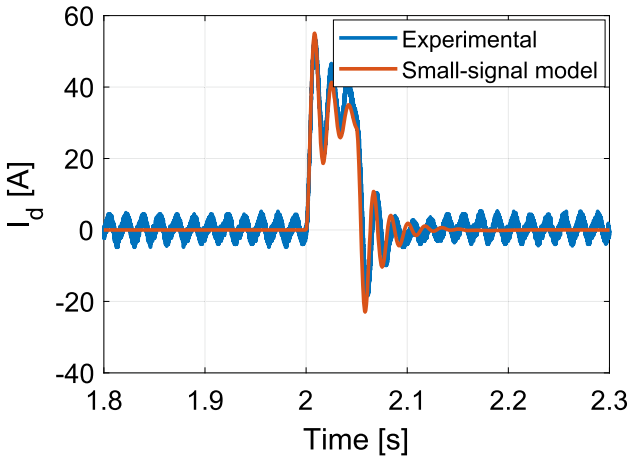

Fig. 18 Small signal x experimental synchronverter result: current i_d under a 5% disturbance in the d-axis component of the bus voltage for 50 ms

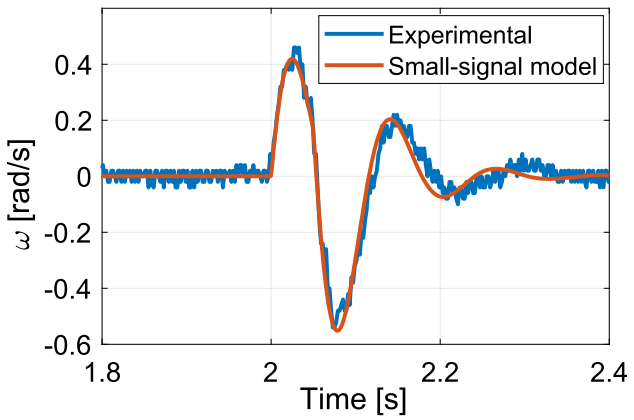

Fig. 19 Small signal × experimental synchronverter result: frequency under a 2 kW disturbance in the active power for 50 ms

9 Conclusion

An increasing interest in control techniques to emulate the operation of synchronous generators by the use of power converters has been observed in recent year, remarkably the droop control and the synchronverter. In this paper, these two techniques were evaluated and compared in terms of dynamic operation based on small-signal models.

The small-signal models developed explicitly show that the difference between the two control structures can be represented by a 2×2 matrix, which can easily be obtained also for other control algorithms for power converters emulating synchronous machines. The results presented showed that for a considerable range of gains, both control algorithms lead to very similar dynamic responses. However, it was also shown that the synchronverter allows an extended range of gains in the stable region, which gives this control algorithm more flexibility. The simplicity of the droop control and its more damped dynamic response can be seen as its main advantages over the synchronverter.

Acknowledgements This work has been supported by the Brazilian agencies CAPES, FAPEMIG and CNPq. The authors also would like to thank the Graduate Program of Electrical Engineering of the Federal University of Minas Gerais, Brazil, the Federal Institute of Minas Gerais, Brazil, and the Wisconsin Electric Machines and Power Electronics Consortium (WEMPEC), from the University of Wisconsin–Madison, USA.

References

Blaabjerg, F., Chen, Z., & Kjaer, S. B. (2004). Power electronics as efficient interface in dispersed power generation systems. *IEEE Transactions on Power Electronics*, *19*(5), 1184–1194. https://doi.org/10.1109/TPEL.2004.833453.

Blaabjerg, F., Teodorescu, R., Liserre, M., & Timbus, A. V. (2006). Overview of control and grid synchronization for distributed power generation systems. *IEEE Transactions on Industrial Electronics*, *53*(5), 1398–1409. https://doi.org/10.1109/TIE.2006.881997.

Bouzid, A. M., Guerrero, J. M., Cheriti, A., Bouhamida, M., Sicard, P., & Benghanem, M. (2015). A survey on control of electric power distributed generation systems for microgrid applications. *Renewable and Sustainable Energy Reviews*, *44*, 751–766.

Brabandere, K. D., Bolsens, B., Keybus, J. V. D., Driesen, J., Prodanovic, M., & Belmans, R. (2005). Small-signal stability of grids with distributed low-inertia generators taking into account line phasor dynamics. In *CIRED 2005—18th international conference and exhibition on electricity distribution* (pp. 1–5). https://doi.org/10.1049/cp:20051273.

Carrasco, J. M., Franquelo, L. G., Bialasiewicz, J. T., Galvan, E., PortilloGuisado, R. C., Prats, M. A. M., et al. (2006). Power-electronic systems for the grid integration of renewable energy sources: A survey. *IEEE Transactions on Industrial Electronics*, *53*(4), 1002–1016. https://doi.org/10.1109/TIE.2006.878356.

Chandorkar, M. C., Divan, D. M., & Adapa, R. (1993). Control of parallel connected inverters in standalone AC supply systems. *IEEE Transactions on Industry Applications*, *29*(1), 136–143. https://doi.org/10.1109/28.195899.

Chen, Y., Hesse, R., Turschner, D., & Beck, H. P. (2011). Improving the grid power quality using virtual synchronous machines. In *2011 international conference on power engineering, energy and electrical drives* (pp. 1–6). https://doi.org/10.1109/PowerEng.2011.6036498.

Coelho, E. A. A., Cortizo, P. C., & Garcia, P. F. D. (2002). Small-signal stability for parallel-connected inverters in stand-alone AC supply systems. *IEEE Transactions on Industry Applications*, *38*(2), 533–542. https://doi.org/10.1109/28.993176.

Ferreira, R. V., Silva, S. M., Brandao, D. I., & Antunes, H. M. A. (2016). Single-phase synchronverter for residential PV power systems. In *2016 17th international conference on harmonics and quality of power (ICHQP)* (pp. 861–866). https://doi.org/10.1109/ICHQP.2016.7783378.

Frack, P. F., Mercado, P. E., & Molina, M. G. (2015). Extending the visma concept to improve the frequency stability in microgrids. In *2015 18th international conference on intelligent system application to power systems (ISAP)* (pp. 1–6). https://doi.org/10.1109/ISAP.2015.7325530.

Guerrero, J. M., Matas, J., de Vicuna, L. G., Castilla, M., & Miret, J. (2007). Decentralized control for parallel operation of distributed generation inverters using resistive output impedance. *IEEE Transactions on Industrial Electronics*, *54*(2), 994–1004. https://doi.org/10.1109/TIE.2007.892621.

Hossain, E., Kabalci, E., Bayindir, R., & Perez, R. (2014). Microgrid testbeds around the world: State of art. *Energy Conversion and Management*, *86*, 132–153.

Kawabata, T., & Higashino, S. (1988). Parallel operation of voltage source inverters. *IEEE Transactions on Industry Applications*, *24*(2), 281–287. https://doi.org/10.1109/28.2868.

Krishnamurthy, S., Jahns, T. M., & Lasseter, R. H. (2008). The operation of diesel gensets in a CERTS microgrid. In *2008 IEEE Power and Energy Society general meeting—Conversion and delivery of electrical energy in the 21st century* (pp. 1–8). https://doi.org/10.1109/PES.2008.4596500.

Kroposki, B., Lasseter, R., Ise, T., Morozumi, S., Papathanassiou, S., & Hatziargyriou, N. (2008). Making microgrids work. *IEEE Power and Energy Magazine*, *6*(3), 40–53. https://doi.org/10.1109/MPE.2008.918718.

Lasseter, R. H. (2002). Microgrids. In *2002 IEEE Power Engineering Society winter meeting. Conference proceedings (Cat. No.02CH37309)* (Vol. 1, pp. 305–308). https://doi.org/10.1109/PESW.2002.985003.

Lasseter, R. H., & Paigi, P. (2004). Microgrid: A conceptual solution. In *PESC Record—IEEE annual power electronics specialists conference* (Vol. 6, pp. 4285–4290). https://doi.org/10.1109/PESC.2004.1354758.

Lee, C. T., Chuang, C. C., Chu, C. C., & Cheng, P. T. (2009). Control strategies for distributed energy resources interface converters in the low voltage. In *Microgrid IEEE energy conversion congress and exposition (ECCE), 2009* (Vol. 2, pp. 2022–2029). https://doi.org/10.1109/ECCE.2009.5316407.

Liu, Z., Liu, J., Boroyevich, D., Burgos, R., & Liu, T. (2016). Small-signal terminal-characteristics modeling of three-phase droop-controlled inverters. In *2016 IEEE energy conversion congress and exposition (ECCE)* (pp. 1–7). https://doi.org/10.1109/ECCE.2016.7855449.

Ma, Z., Zhong, Q.C., & Yan, J.D. (2012). Synchronverter-based control strategies for three-phase PWM rectifiers. In *2012 7th IEEE conference on industrial electronics and applications (ICIEA)* (pp. 225–230). https://doi.org/10.1109/ICIEA.2012.6360727.

Majumder, R., Chaudhuri, B., Ghosh, A., Majumder, R., Ledwich, G., & Zare, F. (2010). Improvement of stability and load sharing in an autonomous microgrid using supplementary droop control loop. *IEEE Transactions on Power Systems*, *25*(2), 796–808. https://doi.org/10.1109/TPWRS.2009.2032049.

Mariam, L., Basu, M., & Conlon, M. F. (2013). A review of existing microgrid architectures. *Journal of Engineering*, *2013*, 1–8.

Mendoza-araya, P. A. (2014). *Impedance matching based stability criteria for ac microgrids*. Ph.D. Thesis, University of Wisconsin - Madison.

Mishra, S., Pullaguram, D., Buragappu, S. A., & Ramasubramanian, D. (2016). Single-phase synchronverter for a grid-connected roof top photovoltaic system. *IET Renewable Power Generation*, *10*(8), 1187–1194. https://doi.org/10.1049/iet-rpg.2015.0224.

Moslemi, R., & Mohammadpour, J. (2015). Accurate reactive power control of autonomous microgrids using an adaptive virtual inductance loop. *Electric Power Systems Research*, *129*, 142–149. https://doi.org/10.1016/j.epsr.2015.08.001.

Novotny, D. W., & Lipo, T. A. (1996). *Vector control and dynamics of AC drives*. Oxford: Clarendon Press.

Patrao, I., Figueres, E., Garcerá, G., & González-Medina, R. (2015). Microgrid architectures for low voltage distributed generation. *Renewable and Sustainable Energy Reviews*, *43*, 415–424.

Pogaku, N., Prodanovic, M., & Green, T. C. (2007). Modeling, analysis and testing of autonomous operation of an inverter-based microgrid. *IEEE Transactions on Power Electronics*, *22*(2), 613–625. https://doi.org/10.1109/TPEL.2006.890003.

Rocabert, J., Luna, A., Blaabjerg, F., & Rodríguez, P. (2012). Control of power converters in AC microgrids. *IEEE Transactions on Power Electronics*, *27*(11), 4734–4749. https://doi.org/10.1109/TPEL.2012.2199334.

Rowe, C., & Summers, T. (2013). Implementing the virtual output impedance concept in a three phase system utilising cascaded PI controllers in the DQ rotating reference frame for microgrid inverter. In *Proceedings of 15th European power electronics conference—EPE 2013* (pp. 1–10).

Sao, C. K., & Lehn, P. W. (2008). Control and power management of converter fed microgrids. *IEEE Transactions on Power Systems*, *23*(3), 1088–1098. https://doi.org/10.1109/TPWRS.2008.922232.

Shintai, T., Miura, Y., & Ise, T. (2014). Oscillation damping of a distributed generator using a virtual synchronous generator. *IEEE Transactions on Power Delivery*, *29*(2), 668–676. https://doi.org/10.1109/TPWRD.2013.2281359.

Skjellnes, T., Skjellnes, A., & Norum, L. (2002). Load sharing for parallel inverters without communication. In *Proceedings of NORPIE* (August):12–14. http://www.elkraft.ntnu.no/eno/Papers2002/Load-sharing-norpie02.pdf.

Tayab, U. B., Roslan, M. A. B., & Hwai, L. J. (2016). Kashif M (2017) A review of droop control techniques for microgrid. *Renewable and Sustainable Energy Reviews*, *76*, 717–727. https://doi.org/10.1016/j.rser.2017.03.028.

Wei, Z., Jie, C., & Chunying, G. (2015). Small signal modeling and analysis of synchronverters. In *2015 IEEE 2nd international future energy electronics conference (IFEEC)* (pp. 1–5). https://doi.org/10.1109/IFEEC.2015.7361434.

Wen, B., Boroyevich, D., Burgos, R., Mattavelli, P., & Shen, Z. (2016). Analysis of D–Q small-signal impedance of grid-tied inverters. *IEEE Transactions on Power Electronics*, *31*(1), 675–687. https://doi.org/10.1109/TPEL.2015.2398192.

Zhang, C. H., Zhong, Q. C., Meng, J. S., Chen, X., Huang, Q., Chen, S., et al.(2013). An improved synchronverter model and its dynamic behaviour comparison with synchronous generator. In *2nd IET renewable power generation conference (RPG 2013)* (pp. 1–4). https://doi.org/10.1049/cp.2013.1879.

Zhang, G., Jin, Z., Li, N., Hu, X., & Tang, X. (2014). A novel control strategy for parallel-connected converters in low voltage microgrid. In *IEEE transportation electrification conference and expo, ITEC Asia-Pacific 2014—Conference proceedings*. https://doi.org/10.1109/ITEC-AP.2014.6941246.

Zhong, Q., Member, S., & Weiss, G. (2011). Synchronverters: Grid-friendly inverters that mimic synchronous generators. *Control of Power Inverters in Renewable Energy and Smart Grid Integration*, *58*(4), 1259–1267. https://doi.org/10.1002/9781118481806.ch18.

Zhong, Q. C., Nguyen, P. L., Ma, Z., & Sheng, W. (2014). Self-synchronized synchronverters: Inverters without a dedicated synchronization unit. *IEEE Transactions on Power Electronics*, *29*(2), 617–630. https://doi.org/10.1109/TPEL.2013.2258684.